Solar Energy Materials & Solar Cells 155 (2016) 20–29

Contents lists available at ScienceDirect

Solar Energy Materials & Solar Cells

journal homepage: www.elsevier.com/locate/solmat

Tailoring band structure of ternary CdS_xSe_{1-x} quantum dots for highly efficient sensitized solar cells

Ru Zhou [a,b,*], Lei Wan [a], Haihong Niu [a], Lin Yang [b], Xiaoli Mao [a], Qifeng Zhang [b], Shiding Miao [a], Jinzhang Xu [a], Guozhong Cao [b,**]

[a] School of Electrical Engineering and Automation, Hefei University of Technology, Hefei 230009, Anhui Province, PR China
[b] Department of Materials Science and Engineering, University of Washington, Seattle, WA 98195, USA

ARTICLE INFO

Article history:
Received 9 October 2015
Received in revised form
28 March 2016
Accepted 28 April 2016

Keywords:
Solar cells
Ternary quantum dot
Graded band structure
Interfacial defects

ABSTRACT

Instead of employing numerous binary quantum dots (QDs), engineering ternary alloyed ones has been emerging as a promising approach to tailor their optical and electronic properties. In this paper, composition-tunable CdS_xSe_{1-x} QDs have been explored and demonstrated to be efficient sensitizers for quantum dot-sensitized solar cells (QDSCs). The optical bandgap and the corresponding band edges could be varied by controlling the component ratios of the ternary QDs while keeping the particle size constant, and a moderate bandgap was attained to deliver broad light harvesting and ideal band alignment. The successful balance of these two requirements resulted in a power conversion efficiency (PCE) of 3.58% for CdS_xSe_{1-x} QD-sensitized TiO_2 solar cells. When the engineered CdS_xSe_{1-x} interlayer was further incorporated between CdS core and CdSe shell layers, a superior PCE of 5.06% has been reached for the graded CdS/CdS_xSe_{1-x}/CdSe structure, which appreciably outperforms the conventional CdS/CdSe one (η=4.41%). The incorporation of CdS_xSe_{1-x} interlayer offers two benefits, (1) the construction of a favorable stepwise band structure, facilitating desired charge injection, and (2) the passivation of the interfacial defects and interphase strain, contributing to suppressed charge recombination. This work highlights the broad prospect of ternary alloyed QDs for developing highly efficient QDSCs.

1. Introduction

The pressing demand of cost-effective and highly efficient solar devices for clean and sustainable energy, to partially replace fossil fuels has been intensified with an increasing concerns of environmental pollution and climate change all over the world [1,2]. Inorganic semiconductor quantum dot-sensitized solar cells (QDSCs) with rapid enhanced power conversion efficiency recently have received revitalized attention as third generation photovoltaic cells due to the versatile advantages of quantum dots (QDs) compared to the conventional dye sensitizers, such as tunable bandgap by controlling their size, large extinction coefficient, multi-excition generation, and high stability toward water and oxygen [3–18]. A theoretical power conversion efficiency (PCE) up to 44%, beyond the traditional Shockley and Queisser limit of 32% for semiconductor solar cells, has encouraged researchers to develop QDSCs with the use of a variety of QDs as sensitizers for light harvesting, including CdS [13], CdSe [14], CdTe [16], PbS [17], PbSe [18], etc. Compared to the metal halide perovskites as light harvesters, which have stunned the photovoltaic community with a PCE exceeding 20% but suffered from moisture-sensitive nature, inorganic QDs show impressive stability to ambient conditions [1]. Among kinds of the QDs developed, the fascinating CdS/CdSe co-sensitization system has been shown to demonstrate the excellent power conversion efficiencies (PCEs) over 5% employing mesoporous TiO_2 films [6,19,20]. Our previous work also report an outperforming PCE of 6.33% for CdS/Mn-CdSe sensitized TiO_2 solar cell [19].

In QDSCs, the optical bandgap of the QDs and the alignment of their bands with the underlying oxide semiconductor are critical for broad light harvesting and efficient charge separation [21]. However, these two requirements are not easily fulfilled simultaneously. Although the utilization of QDs with large size or narrow bandgap can expand the light absorption spectrum, the low conduction band edge of those QDs may prevent the effective

* Corresponding author at: School of Electrical Engineering and Automation, Hefei University of Technology, Hefei 230009, Anhui Province, PR China. Tel.: +86 551 62904156; fax: +86 551 62904156.
** Corresponding author. Department of Materials Science and Engineering, University of Washington, Seattle, WA 98195, USA. Tel.: +1 206 616 9084; fax: +1 206 543 3100.
E-mail addresses: zhouru@hfut.edu.cn (R. Zhou), gzcao@u.washington.edu (G. Cao).

http://dx.doi.org/10.1016/j.solmat.2016.04.049
0927-0248/

injection of photo-generated electrons from the QD sensitizer into oxide semiconductor. This explains the relatively low PCEs of narrow bandgap QDs (such as PbS and Ag_2S) sensitized solar cells, which possessed broad light harvesting, but suppressed electron injection [22,23]. Therefore, under such circumstance, the tuning of optical and electronic properties of QDs purely by changing the particle size could be limited. Fortunately, instead of employing binary QDs, tailoring ternary QDs through alloying has emerged as a promising approach to pursue desired bandgap while keeping the particle size constant [24]. The optical bandgap and the corresponding band edges can be feasibly varied by altering component ratios of the alloyed QDs at a fixed size. In other words, in addition to size, ternary QDs provide composition as an additional dimension for tailoring their optical and electronic properties. Hence, employing composition-tunable alloyed QDs as sensitizer enables us to improve the optical absorption without overly impeding the subsequent charge injection from QDs to oxide semiconductors [25]. However, in contrast to the use of numerous binary QDs, the attempts to explore ternary alloyed ones as sensitizers in liquid-junction QDSCs to manipulate the band structure have been relatively rare [9,21,26–29].

CdS_xSe_{1-x} alloyed semiconductors belong to ternary chalcogenide compounds, and the bandgap can be engineered between the bulk CdS (2.45 eV) and CdSe (1.75 eV), over a wide visible wavelength range [29]. Moreover, CdS and CdSe are considerably miscible in view of their small lattice mismatch, leading to the formation of CdS_xSe_{1-x} ($0 \le x \le 1$) solid solution with almost zero enthalpy change [30]. Not surprisingly, the excellent ternary alloyed QDs attracted significant interest in the potential photovoltaic application. Up to now, much work has been committed to the preparation of different morphologies of ternary CdS_xSe_{1-x}, such as colloidal QDs [24], thin film [29], nanobelt [31], etc., and the optical and electrical properties have been extensively studied. Hossain et al. reported a PCE of 4.05% based on CdS_xSe_{1-x} sensitized TiO_2 solar cell, rivalling the well-studied cascaded CdS/CdSe photoelectrodes [21]. Sung et al. synthesized complete composition-tuned CdS_xSe_{1-x} layer sensitized TiO_2 nanowire arrays, and employed as efficient photoelectrodes for hydrogen generation [29].

In this work, CdS_xSe_{1-x} QDs with controlled composition were prepared as the sensitizers for QDSCs by successive ionic layer adsorption and reaction (SILAR), instead of the high-temperature thermal vapor transport or hot injection methods [24,29]. SILAR allows the CdS_xSe_{1-x} layer to successively grow in a reproducible and controllable manner [13]. Aiming to engineer novel band alignment facilitating charge separation and impair the interfacial defects and interphase strain for suppressed charge recombination in the multilayered QDSCs, CdS_xSe_{1-x} interlayer was further incorporated into CdS/CdSe co-sensitization system between CdS core and CdSe shell for enhanced photovoltaic performance. Such an idea is similar to that of boosting the luminescence quantum efficiency by gradually changing the shell composition in multi-shell structures [32,33]. Ultimately, the graded CdS/CdSSe/CdSe structure delivers a superior PCE of 5.06% under simulated AM 1.5 100 mW cm^{-2} illumination, which turns out to outperform the conventional CdS/CdSe QDSCs (η=4.76%) prepared under the same manufacturing procedures.

2. Experimental

2.1. Chemicals and materials

Titanium oxide (TiO_2, Degussa, P25), α-terpineol ($C_{10}H_{18}O$, 96%, Sigma Aldrich), ethyl cellulose ($[C_6H_7O_2(OC_2H_5)_3]_n$, 48.0–49.5% (w/w) as ethoxyl, Sigma Aldrich), cadmium acetate dihydrate ($Cd(CH_3COO)_2 \cdot 2H_2O$, 98%, Sigma Aldrich), sodium sulfide nonahydrate ($Na_2S \cdot 9H_2O$, $\geq$98.0%, Sigma Aldrich), sulfur (S, purified by sublimation, Sigma Aldrich), sodium sulfide anhydrous (Na_2SO_3, 99.1%, Italy), trisodium salt of nitrilotriacetic acid ($N(CH_2COONa)_3$, $\geq$98.0%, Aldrich), zinc acetate dihydrate ($Zn(CH_3COO)_2 \cdot 2H_2O$, $\geq$99.0%, Aldrich), selenium powder (Se, 99.5%, Alfa Aesar), brass foil (alloy 260, 0.3 mm thick, Alfa Aesar), hydrochloric acid (HCl, 37%, USA), methanol (CH_3OH, $\geq$99.5%, Sigma Aldrich), and ethanol (CH_3COOH, $\geq$99.5%, Decon) were all used as received.

2.2. Preparation of mesoporous TiO_2 films

Commercially available F-doped tin oxide (FTO) glass was used as transparent conducting substrates to prepare TiO_2 photoelectrodes. To prepare TiO_2 paste, 0.5 g Degussa P25 mixed with 0.25 g ethyl cellulose and 1.75 g α-terpineol were first dispersed into 5.0 mL ethanol, and then sonicated for 30 min to form a slurry after removing the ethanol under stirring. Mesoporous TiO_2 films were prepared by doctor blading of TiO_2 paste on the clean FTO substrate, followed by sintered at 500 °C for 30 min in air with a heating rate of 5 °C/min. The thickness of the TiO_2 film, measured from the cross sectional image of SEM, was ca. 16 μm, as shown in Fig. S1 (ESI†). The active area of the TiO_2 films was approximately 0.36 cm^2 (0.6 cm × 0.6 cm square).

2.3. In situ assembling of QDs

For in situ assembling of QDs by both successive ionic layer adsorption and reaction (SILAR) and chemical bath deposition (CBD) processes, the films were immersed into the as-prepared precursor solutions to allow the ions of the reactants to penetrate into the mesoporous film and incorporate into the interior of mesopores, leading to the formation of one layer of QDs. Specifically, the SILAR processes for CdS_xSe_{1-x} QDs deposition were all conducted inside a glove box under N_2 atmosphere. TiO_2 films were first dipped into cation ion precursor, *i.e.*, 0.1 M $Cd(CH_3COO)_2 \cdot 2H_2O$ methanol solution for 1 min, rinsed with methanol and dried under N_2 atmosphere for several minutes. Subsequently, the dried films were then dipped into anion precursors for another 1 min to allow S^{2-} and Se^{2-} to react with the pre-adsorbed Cd^{2+}, leading to the formation of the desired ternary CdS_xSe_{1-x} QDs. The above anion precursors were prepared by dissolving different amount of Se powder into a concentration-fixed 0.1 M Na_2S solution containing water and methanol (volume ratio, v/v=1/1) under vigorous stirring. The feed Se molar concentrations were 0, 0.00625, 0.0125, 0.025 and 0.05 M, respectively, *i.e.*, Se/S varied from 0/16, 1/16, 2/16, 4/16 to 8/16. The Se^{2-} generated in this process could stay stably for a period of time in alkaline Na_2S solutions. One deposition cycle was completed by further rinsing and drying. The two-step dipping procedure is termed as one SILAR cycle. A certain number of SILAR cycles were employed to obtain a desired amount of QDs loaded on the TiO_2 films. As follows is a brief description of CBD procedure for the deposition of CdSe: 0.1 M Na_2SeSO_3, 0.1 M $Cd(CH_3COO)_2$, and 0.2 M $N(CH_2COONa)_3$ aqueous solution were mixed together with a volume ratio of 1/1/1, and then the TiO_2 films were vertically immersed into the solution for the assembly of a CdSe layer under dark condition at 24 °C for 3 h. Na_2SeSO_3 solution was prepared by dissolving Se powder in an aqueous solution of Na_2SO_3 at 70 °C for ca. 1 h under vigorous stirring. For the preparation of CdS seed layer, 4 SILAR cycles were conducted, employing 0.1 M $Cd(CH_3COO)_2$ in methanol and 0.1 M Na_2S in a mixture of methanol and water (volume ratio, v/v=1/1) as the cation and anion source, respectively. Finally, all the photoelectrodes were coated with 2 SILAR cycles of ZnS passivation layer, by dipping alternatively into 0.1 M $Zn(CH_3COO)_2$ and 0.1 M Na_2S solutions for 1 min/dip. The deposition of ZnS serves as a tunnel barrier for back charge

transfer at the absorber and TiO_2 interface, which improves the performance and stability of the solar devices.

2.4. Solar cell fabrication

Solar device was assembled by sandwiching the as-prepared photoelectrode and Cu_2S counter electrode using a scotch tape spacer (ca. 50 μm thick) and permeating the assembly with the polysulfide electrolyte. The polysulfide electrolyte employed in this study was composed of 1 M S and 1 M Na_2S in deionized water. The counter electrode was a Cu_2S film fabricated on a brass foil, and the preparation procedure can be described briefly as follows: a brass foil was immersed into 37% HCl solution at ca. 70 °C for 0.5 h, then rinsed with water and dried in air; the etched brass foil was then dipped into the as-prepared polysulfide electrolyte for ca. 5 min, resulting in a black Cu_2S layer forming on the foil.

2.5. Characterization

Morphologies of the film samples were directly characterized by a JEOL JSM 7000 scanning electron microscope (SEM) equipped with an energy dispersion X-ray (EDX) spectrometer to analyze the element content and distribution. Transmission electron microscope (TEM) and high-resolution TEM observations were performed on a Tecnai G2 F20 microscope. Optical absorption spectra were measured on a thermal scientific UV–vis–NIR spectrophotometer (Evolution 300 PC) fitted with an integrating sphere accessory. Photovoltaic properties were measured using an HP 4155A programmable semiconductor parameter analyzer under AM 1.5 simulated sunlight with the power density of 100 mW cm^{-2}. Current density-voltage (*J-V*) characteristics were recorded using a Keithley 2400 source meter with an active cell area of 0.36 cm^2. Electrochemical impedance spectroscopy (EIS) measurements were carried out under dark condition using a Solartron 1287A coupled with a Solartron 1260 FRA/impedance analyzer.

3. Results and discussion

A series of CdS_xSe_{1-x} QDs sensitized TiO_2 films prepared by 10 SILAR cycles with the increasing feed Se molar concentration of 0, 0.00625, 0.0125, 0.025 and 0.05 M are donated as Se/S=0/16, 1/16, 2/16, 4/16 and 8/16 samples, respectively. Fig. 1 shows the surface morphologies of the bare and CdS_xSe_{1-x} QDs sensitized TiO_2 films. It is observed that the bare TiO_2 film exhibited a highly porous nanostructure, and such mesoporous structure allows the penetration of the cationic and anionic precursor solutions. SILAR as a solution deposition method is supposed to be ideal for allowing the infiltration of the reactions into the film pores [12]. With the deposition of CdS_xSe_{1-x} QDs, the mesoporous structure of TiO_2 film was largely retained as shown in Fig. 1(b-f), however small pores were partially filled. Moreover, the particles on the sensitized films become larger and coarser in comparison with the bare TiO_2 film. These observations imply a successful deposition of QDs on the photoelectrodes. Meanwhile, there are no significant differences on the surface morphology between the films sensitized by CdS_xSe_{1-x} QDs of different Se/S ratios.

For microscopically tracing the spatial distribution of QDs in the mesoporous film, the elemental mapping technique was employed. The cross-sectional mapping images (Fig. S1, ESI†) demonstrates that the element distributions of Cd, S and Se are indeed essentially homogeneous throughout the thickness of the mesoporous TiO_2 film, as we have expected.

The actual molar ratio of Se/S for CdS_xSe_{1-x} QDs adsorbed on each film was examined by EDX analysis. The corresponding EDX spectra of the bare and sensitized TiO_2 films are presented in Fig. S2 (ESI†). As shown, the bare TiO_2 film only exhibits the two typical peaks corresponding to Ti and O, whereas for the sensitized films, energy-dispersion peaks corresponding to Cd, S and Se also appear. Fig. 2(a) presents the actual atomic ratios of Se and S on each sample (Se/S=0/16, 1/16, 2/16, 4/16 and 8/16). The obtained Se/S molar ratios are 0, 0.42, 0.76, 1.22 and 1.80 for 0/16, 1/16, 2/16, 4/16 and 8/16 samples, respectively, which showed a corresponding increase along with the increase of the Se concentration during the SILAR deposition. However, it is noteworthy that a deviation between the feed Se/S ratio in the precursor solutions and the actual Se/S ratio in the as-prepared QDs is observed, as demonstrated in Fig. 2(b). For instance, the feed molar ratio of 4/16

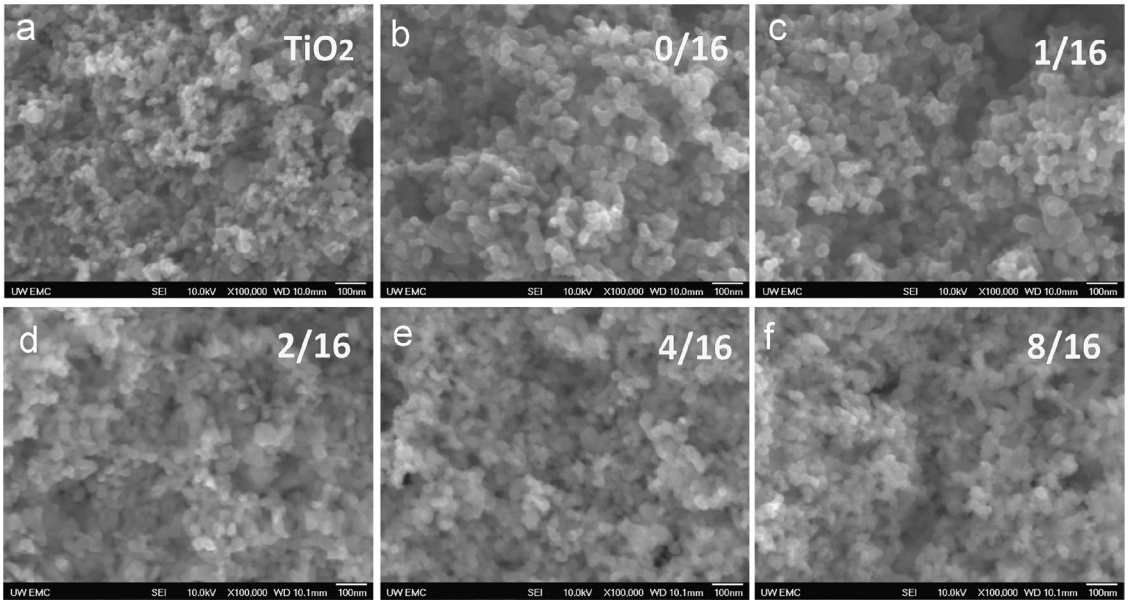

Fig. 1. SEM images of a bare TiO_2 mesoporous film (a), and a series of CdS_xSe_{1-x} QDs sensitized TiO_2 films prepared under the feed molar ratio of Se/S=0/16 (b), 1/16 (c), 2/16 (d), 4/16 (e) and 8/16 (f), respectively.

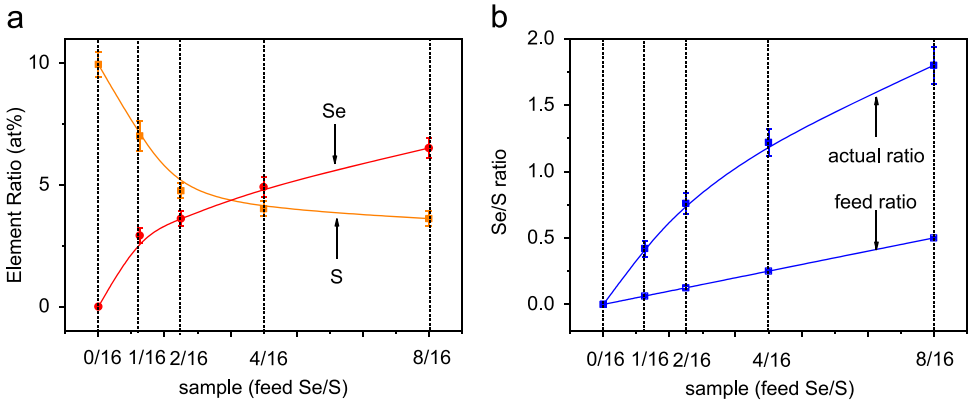

Fig. 2. (a) Element rations of Se and S based on EDX calculations, and (b) the feed molar ratio of Se/S in the precursor solutions versus the actual molar ratio in the as-prepared CdS_xSe_{1-x} QDs.

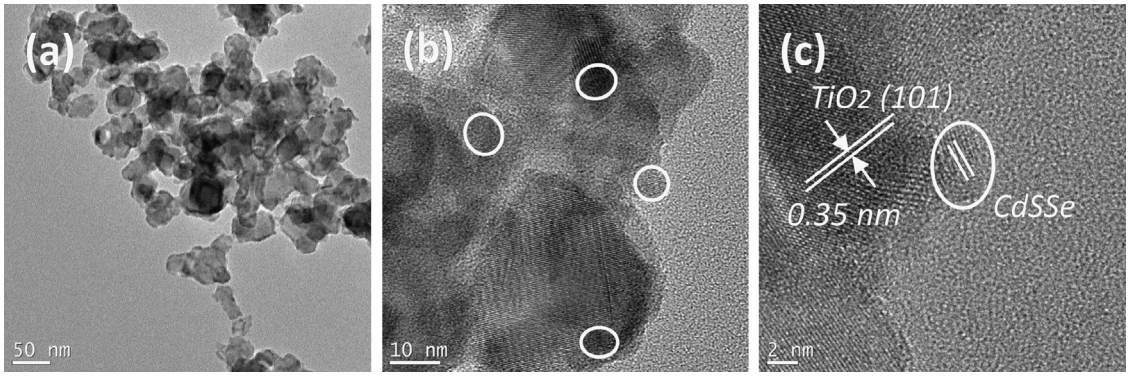

Fig. 3. TEM (a, b) and HRTEM (c) images of CdS_xSe_{1-x} (Se/S=4/16) QDs sensitized TiO_2 nanoparticles. The white ellipse curves in the images denote the SILAR-deposited QDs.

sample is 0.25, while the corresponding QDs deliver an actual ratio of 1.22. Such a phenomenon reveals a different deposition rate for S^{2-} and Se^{2-} to construct the CdS_xSe_{1-x} QDs with Cd^{2+} [24].

The typical TEM images of the as-prepared ternary CdS_xSe_{1-x} QDs (Se/S=4/16 sample) sensitized TiO_2 film are shown in Fig. 3, which further microscopically confirmed the successful loading of QDs on TiO_2 surface. The boundary of regular-shaped TiO_2 nanocrystals appeared obscure since the SILAR-deposited QDs forms as separated small particles randomly distributed on TiO_2, similar to some scenarios reported in literature [17,22,28]. The achieved ellipsoidal QDs are marked by the white ellipse curves in the images. High-resolution TEM (HRTEM) image (Fig. 3(b)) further revealed that the mean particle size of the achieved QDs prepared by SILAR under 10 cycles was ~6 nm, and allowed the identification of the lattice fringes corresponding to anatase TiO_2 and CdS_xSe_{1-x} QDs.

Fig. 4(a) shows the UV–vis absorption spectra of CdS_xSe_{1-x} QDs sensitized TiO_2 mesoporous films. The absorption onset of the successively deposited QDs on TiO_2 film shifted to a longer wavelength along with the increase of Se content in the ternary CdS_xSe_{1-x} QDs. Since the SILAR cycle was set to be the same for all the samples here, the red-shifted absorption onset implies the narrowed bandgap of ternary QDs. The effective bandgap of CdS_xSe_{1-x} QDs can be estimated by extrapolating the linear portion of the $(Ah\upsilon)^2$ versus $h\upsilon$ plots at $A=0$, according to the following equation, which expresses the relationship between the optical bandgap (E_g) for direct inter-band transition and the absorption coefficient (A) near the absorption edge [11,13],

$$(Ah\upsilon)^2 = c(h\upsilon - E_g) \quad (1)$$

where c is a constant, υ is the frequency and h is Planck constant. The obtained values of effective bandgaps and absorption onsets are plotted in Fig. 4(c). As expected, with the increase of Se content in CdS_xSe_{1-x} QDs, the estimated bandgaps become increasingly smaller, correlated with the more and more pronounced red shift of absorption edge. For example, the bandgap of Se/S=4/16 sample is ~2.01 eV, and such a value is considerably larger than the bandgap of bulk CdSe (1.75 eV), while smaller than that of bulk CdS (2.45 eV) [29]. In addition, it is noteworthy here that the Se/S=0/16 sample (*i.e.*, pure CdS sensitized TiO_2 films) exhibits a bandgap of 2.31 eV narrower than 2.42 eV for bulk CdS. Such an anomalous absorption-edge red shift phenomenon has been carefully discussed in our previous work, and probably results from a particularly long absorption tail that extends far into the red region and is amplified by the large optical thickness of high-surface-area mesoporous films [13]. Schematically depicted in Fig. 4(d) is the band structure of CdS_xSe_{1-x} QDs depending on the molar ratio of Se/S as revealed by the corresponding absorption spectra. Therefore, the absorption spectrum and band edge of the achieved ternary CdS_xSe_{1-x} QDs can be readily controlled by altering the composition ratio of Se/S without changing the size of QDs. The flexibility of tailoring the absorption range and band structure makes the composition-tunable alloyed CdS_xSe_{1-x} QDs promising for photovoltaic application. The continuous shift of the absorption edge without obvious humps corresponding to the characteristic absorption shoulders for CdS and CdSe further confirms the formation of homogeneous ternary alloys of tunable compositions instead of a mixture of CdS and CdSe [21].

The photovoltaic characteristics of CdS_xSe_{1-x} QDSCs under one sun illumination (AM 1.5 G, 100 mW cm^{-2}) are presented in Fig. 5, and the short circuit current density (J_{sc}), open circuit voltage (V_{oc}), fill factor (FF) and PCE (η) are summarized in Table 1. It is

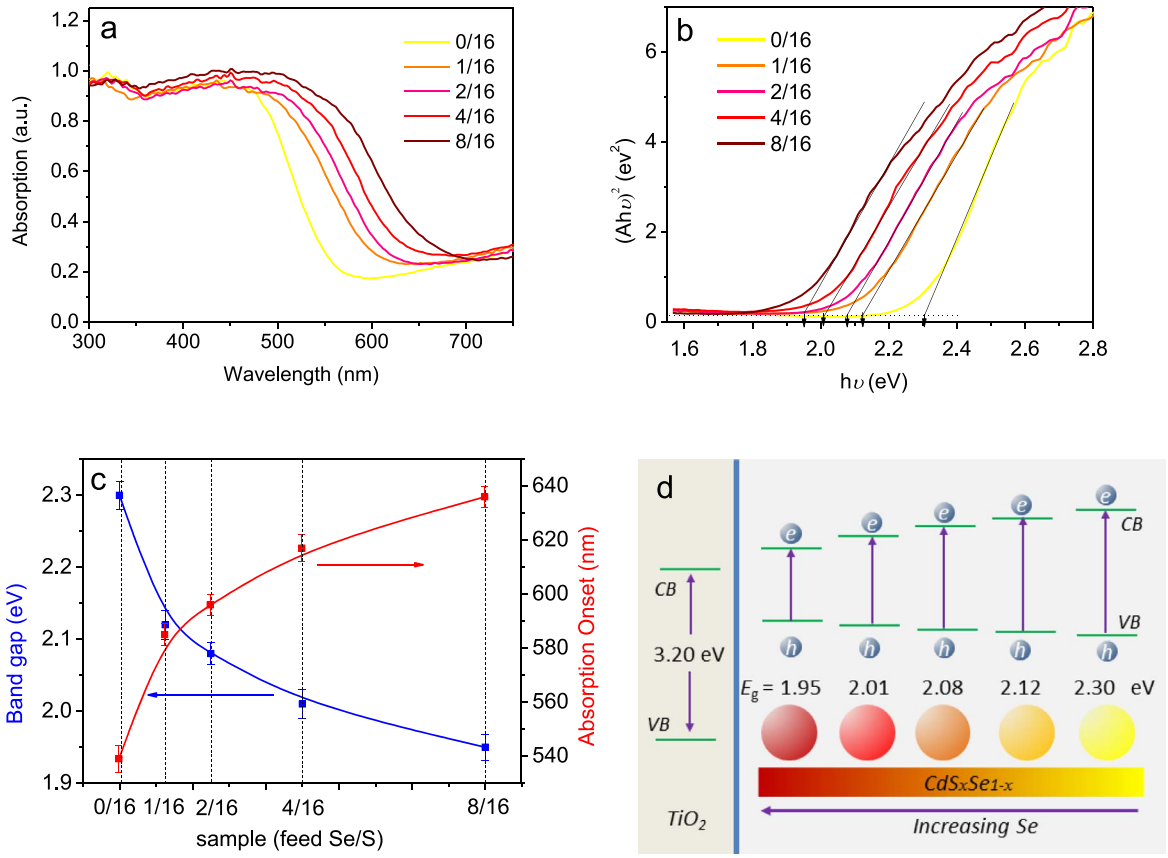

Fig. 4. (a) UV–vis absorption spectra, (b) $(Ah\upsilon)^2$ versus $h\upsilon$ plots, (c) the estimated effective bandgaps and absorption onsets of a series of CdS_xSe_{1-x} sensitized TiO_2 film samples, and (d) schematic diagram depicting the band structures of CdS_xSe_{1-x} QDs depending on the molar ratio of Se/S.

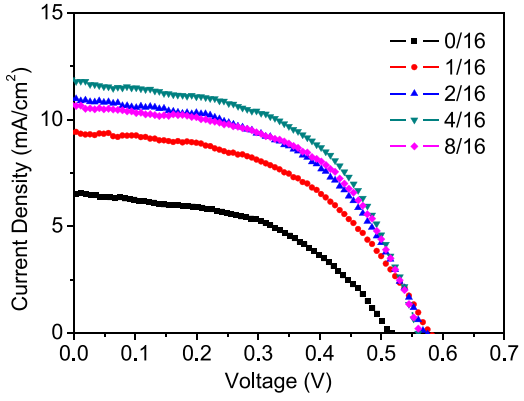

Fig. 5. Current density-voltage (*J-V*) characteristics of QDSCs based on a series of CdS_xSe_{1-x} sensitized TiO_2 photoelectrodes measured under the illumination of one sun (AM 1.5, 100 mW cm^{-2}).

Table 1
Photovoltaic parameters of QDSCs based on a series of CdS_xSe_{1-x} sensitized TiO_2 photoelectrodes.

Sample	J_{sc} (mA cm^{-2})	V_{oc} (V)	FF	η (%)
0/16	6.56(±0.15)	0.51(±0.01)	0.48(±0.01)	1.61(±0.08)
1/16	9.42(±0.18)	0.58(±0.01)	0.49(±0.01)	2.68(±0.10)
2/16	10.99(±0.21)	0.57(±0.01)	0.50(±0.01)	3.13(±0.12)
4/16	11.85(±0.20)	0.56(±0.01)	0.54(±0.01)	3.58(±0.11)
8/16	10.69(±0.20)	0.56(±0.01)	0.55(±0.01)	3.29(±0.11)

worth mentioning that, for each solar device studied in this paper, at least three identical samples have been fabricated to check the reproducibility of cell performance. As shown in Table 1, the PCE first increases and then decreases with the increase of Se content incorporated the alloyed QDs, and the parameters of J_{sc}, V_{oc} and FF are all significantly improved compared to the pure CdS QDSC (*i.e.*, the Se/S=0/16 sample). It is known that increasing Se content in ternary CdS_xSe_{1-x} QDs will broad the light absorption range but lower the conduction band edge of QDs so as to impede the charge injection. The successful balance of these two requirements helps to result in an excellent photovoltaic performance. The solar cell made of the Se/S=4/16 photoelectrode acquires J_{sc} of 11.85 mA cm^{-2}, V_{oc} of 0.56 V, and FF of 0.54, yielding an optimized PCE of 3.58%. Moreover, the performance of a QDSC is very much dependent on SILAR cycle to deposit QDs, as revealed in Fig. S3 (ESI†) and Table S1 (ESI†), which gives the photovoltaic characteristics of CdS_xSe_{1-x} QDSCs (Se/S=4/16 sample) under various SILAR cycles. Specifically, it is easy to understand that a small amount of QDs deposited on the TiO_2 film would result in a small photocurrent density, along with a low PCE; however, an overload of QDs might also result in a poor cell performance, possibly for the reason of the blocking of the mesopores, which leads to a decrease of the QD/electrolyte contact area and unfavorable electron transport at the TiO_2/QD/electrolyte interface [12,13]. This explains the fact that, although the QD loading would further increase, the cell performance deteriorated along with the over-extended SILAR cycle. An optimal SILAR cycle is achieved to be ~10. Hence, to sum up, with the construction of solar cells employing ternary alloyed CdS_xSe_{1-x} QDs, impressive cell performances are achievable relative to those of the constituent binary systems.

Based on the results and discussions above, it is concluded that ternary CdS_xSe_{1-x} QDs are demonstrated to be efficient sensitizers for QDSCs, and furthermore, a moderate bandgap for QD sensitizer is desired to sufficiently match the solar spectrum for broad light

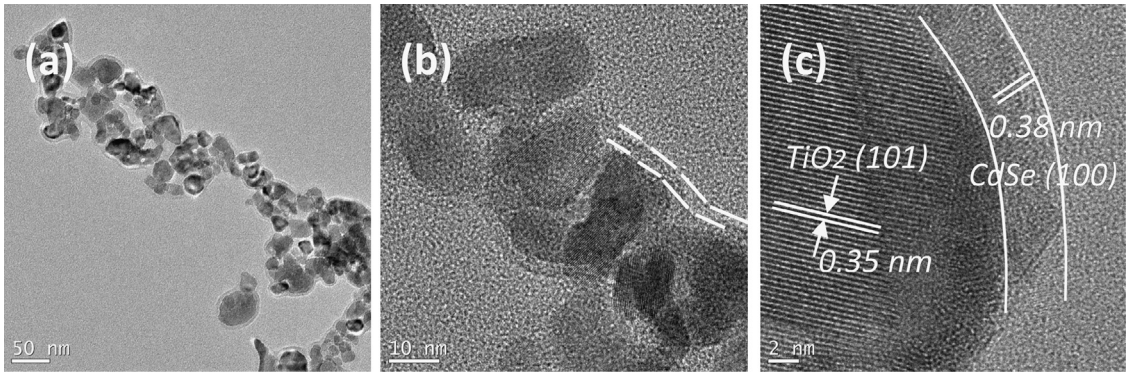

Fig. 6. TEM (a, b) and HRTEM (c) images of CdS/CdSSe/CdSe QDs sensitized TiO_2 nanoparticles. The white curves in the images denote the CBD-deposited thin layer of QDs.

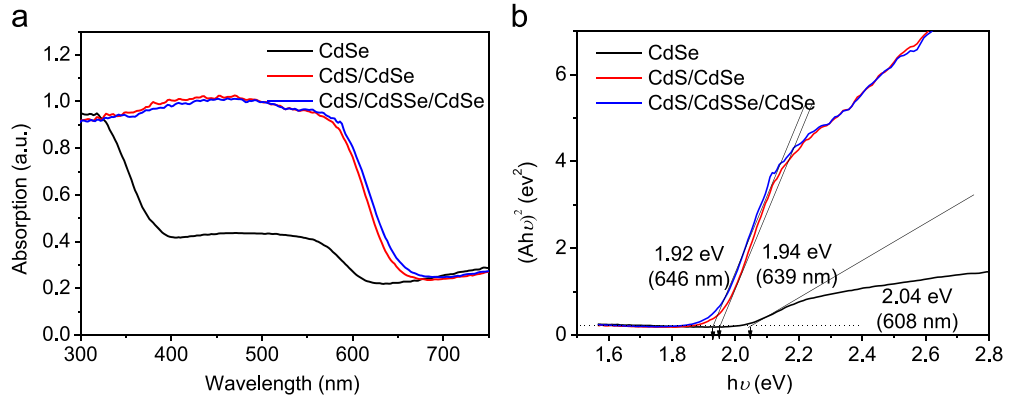

Fig. 7. (a) UV–vis absorption spectra, and (b) $(Ah\upsilon)^2$ versus $h\upsilon$ plots of CdSe, CdS/CdSe and CdS/CdSSe/CdSe sensitized TiO_2 photoelectrodes.

harvesting and achieve ideal band alignment for efficient charge separation. Aiming to expand its applications for enhanced photovoltaic performance, the engineered ternary CdS_xSe_{1-x} QDs were further incorporated into CdS/CdSe co-sensitization system as an interlayer. Here it should be noted that the ternary QDs mentioned below are prepared under the feed molar ratio of Se/S=4/16 (hereinafter referred to as "CdSSe"). It is expected that CdSSe interlayer would engineer novel band alignment for efficient charge separation as well as impair the interfacial defects and interphase strain at CdS/CdSe interface.

For the construction of the CdS/CdSSe/CdSe multilayer structure, the CdS core and CdSe shell layer were prepared by SILAR and CBD, respectively. The deposition status of the multilayered QDs on TiO_2 was also microscopically examined by TEM images as shown in Fig. 6. Obviously, the QDs are successfully loaded on the TiO_2 surface. However, different from that of SILAR deposited CdSSe QDs that forms small separated particles as revealed in Fig. 3, the CdS/CdSSe/CdSe structure ensures a conformal coverage of the thin layer coated continuously on TiO_2. Such a difference in morphology is closely correlated with the deposition strategy of QDs, which has been carefully demonstrated in our previous work [12]. That is, in contrast with layer-by-layer growth based on a SILAR process, CBD is a simple one-pot strategy for obtaining well-covered QDs layer. In our experimental process to prepare CdSe shell by CBD, the application of sodium selenosulfite (Na_2SeSO_3) allows the slow generation of Se anions, which is useful for rate control to prevent aggregation and achieve uniform QDs [34]. The achieved conformal coverage for CdS/CdSSe/CdSe multishell electrode are expected to result in an interfacial structure with superior ability to inhibit the charge recombination at TiO_2/electrolyte interface, thus contributing for the performance improvements of the corresponding cells.

Fig. 7 presents the UV–vis absorption spectra of CdSe, CdS/CdSe and CdS/CdSSe/CdSe sensitized TiO_2 films. The light harvesting capability, as one of the key functional properties of a sensitized film, can be evaluated employing the UV–vis absorption spectrum, which highlights two important features, the absorbance and absorption range. The absorbance is determined by the amount of QDs loaded while the absorption range is usually bound up with the intrinsic bandgap and particle size of the QDs. As reflected in Fig. 7(a), compared to the pure CdSe sample, the presence of the pre-assembled CdS or CdSSe seed layer underneath CdSe significantly enhances the subsequent growth of CdSe prepared by CBD, as demonstrated by the higher absorbance and broader absorption range for CdS/CdSe and CdS/CdSSe/CdSe samples. Moreover, the CdS/CdSe and CdS/CdSSe/CdSe sensitized films show almost the same absorbance, while the latter exhibits a slightly broader light absorption range with an absorption onset at a wavelength of ca. 646 nm, longer than that of 639 nm for the former (as illustrated in Fig. 7(b)). The results indicate that although the comparable amount of QDs loaded is achieved for both CdS/CdSe and CdS/CdSSe/CdSe samples, the incorporated CdSSe interlayer as the seed layer may promote the grain growth of the subsequent CBD-deposited CdSe, which is probably due to the impaired lattice mismatch at the CdS/CdSe interface.

CdSe, CdS/CdSe and CdS/CdSSe/CdSe QDSCs were fabricated employing the corresponding sensitized TiO_2 photoelectrodes. It is well known that the interface charge recombination plays a leading role compared to the bulk recombination for sensitized nanocrystalline solar cells, and the interface charge recombination pathways mainly include the back reaction of the injected electrons in the CB of QDs and TiO_2 with the electron acceptors in the electrolyte and the recombination of these electrons with holes remaining in the VB of QDs, respectively [2,12]. In order to evaluate the interfacial charge recombination processes in the solar

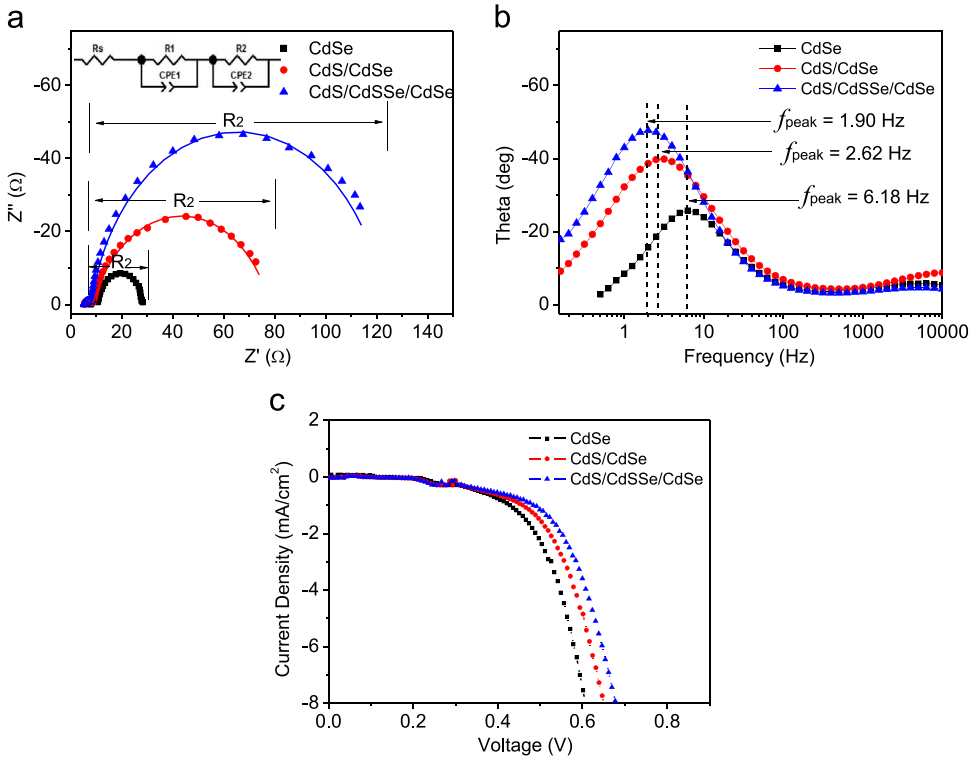

Fig. 8. (a) Nyquist plots and (b) Bode plots of EIS spectra of CdSe, CdS/CdSe and CdS/CdSSe/CdSe QDSCs recorded under dark conditions at an applied forward bias of −0.6 V, and (c) *J-V* characteristics CdSe, CdS/CdSe and CdS/CdSSe/CdSe QDSCs measured under dark conditions.

Table 2
Electrochemical impedance results of CdSe, CdS/CdSe and CdS/CdSSe/CdSe QDSCs recorded under dark conditions at an applied forward bias of −0.6 V.

Sample	R_s (Ω)	R_1 (Ω)	R_2 (Ω)	τ_n (ms)
CdSe	7.8(±2.12)	3.1(±1.01)	17.6(±3.85)	25.8(±1.62)
CdS/CdSe	5.4(±2.00)	3.4(±1.05)	69.5(±14.02)	60.8(±4.07)
CdS/CdSSe/CdSe	5.2(±1.96)	2.9(±1.00)	115.2(±20.15)	83.8(±6.18)

device, EIS measurements have been carried out. The impedance spectra shown in Fig. 8(a, b) were recorded under dark at an applied forward bias of −0.6 V, and the curves were fitted in terms of the equivalent circuit depicted in the inset of Fig. 8(a). R_s accounts for the sheet resistance of FTO and the contact resistance between FTO and TiO_2, and two typical semicircles in the Nyquist plots of QDSCs correspond to the redox reaction at the counter electrode/electrolyte interface at high frequencies (R_1, smaller semicircle), and the electron transfer at the TiO_2/QD/electrolyte interface at medium frequencies (R_2, bigger semicircle), respectively [35–38]. The fitting results of R_s, R_1 and R_2 for QDSCs based on EIS measurements are presented in Table 2. In consideration of the same electrolyte and counter electrode employed in our experiments, R_1 exhibits no apparent differences for three cells; while for our interest, we would like to draw attention to the most conspicuous difference between the cells, *i.e.*, R_2, which reflects the charge recombination at the TiO_2/QD/electrolyte interface. As shown in Table 2, the R_2 of CdS/CdSSe/CdSe cell is estimated to be 115.2 Ω, which is remarkably larger than that of CdS/CdSe cell (69.5 Ω). The fact revealed that, compared to CdS/CdSe, electrons in CdS/CdSSe/CdSe photoelectrode are more difficult to recombine with the electrolyte redox couple (S^{2-}/S_n^{2-}) in view of the higher value of R_2. Since the same counter electrode, electrolyte and TiO_2 film were employed for the cells, the value difference of R_2 should be closely bound up with the features of QDs deposited onto the TiO_2 surface, which could give rise to different charge transport and recombination characteristics. Evidently, the engineered CdS/CdSSe/CdSe multishell structure should attribute to the much smaller recombination resistance value associated with the suppression of charger recombination in the solar device [35]. Meanwhile, not surprisingly, the R_2 of CdSe cell prepared without the pre-assembled CdS or CdSSe layer is further smaller (17.6 Ω), indicating the more serious charge recombination. Fig. 8(b) gives the Bode plots of the impedance spectra. The electron lifetime (τ_n) in the TiO_2 can be evaluated by the peak frequency at the minimum phase angle in the Bode plot based on the following equation [38,39]:

$$\tau_n = \frac{1}{\omega_{peak}} = \frac{1}{2\pi f_{peak}} \quad (2)$$

The estimated electron lifetime of CdS/CdSSe/CdSe cell is up to 83.8 ms, much longer than that of 60.8 ms for CdS/CdSe cell. Apparently, the long-lived charge carrier implies a suppressed charge recombination, and ensures the efficient collection of electrons at the FTO substrate. The inference based on EIS analysis is further supported by the *J-V* characteristics measured under dark conditions (Fig. 8(c)), which shows a smallest dark current for the CdS/CdSSe/CdSe cell. Therefore, the CdSSe interlayer is effective in suppressing interface charge recombination.

The photovoltaic characteristics of CdSe, CdS/CdSe and CdS/CdSSe/CdSe QDSCs measured under the illumination of one sun (AM 1.5, 100 mW cm^{-2}) are compared in Fig. 9 and the extracted parameters (*i.e.*, J_{sc}, V_{oc}, FF and η) are tabularized in Table 3. EQE measurement was also performed to cross check and validate our J_{sc} data (see the supplementary information for a detailed calculation and analysis, Fig. S4, ESI†). Apparently, the pure CdSe sensitized solar cell exhibits a much lower J_{sc}, compared to the other two prepared employing pre-assembled seed layers (*i.e.*, CdS and CdSSe), and it is easy to understand here that a low QD loading should be responsible for the small photocurrent density, along with a poor cell performance. Next, for our interest, we would like to pay particular attention to a comparison

between CdS/CdSe and CdS/CdSSe/CdSe cell. As shown, a PCE up to 5.06% has been achieved for CdS/CdSSe/CdSe cell, which is appreciably higher than 4.41% for the commonly studied CdS/CdSe cell. Through the careful comparison of the photovoltaic parameters, relatively larger values of J_{sc} and V_{oc} have been consistently delivered for CdS/CdSSe/CdSe cell, in comparison with CdS/CdSe cell. Since the light absorption capability exhibits no much difference for both CdS/CdSe and CdS/CdSSe/CdSe photoelectrodes, the origin of the difference in photovoltaic performance relies on the charge transfer processes after photocarrier generation: charge injection and recombination.

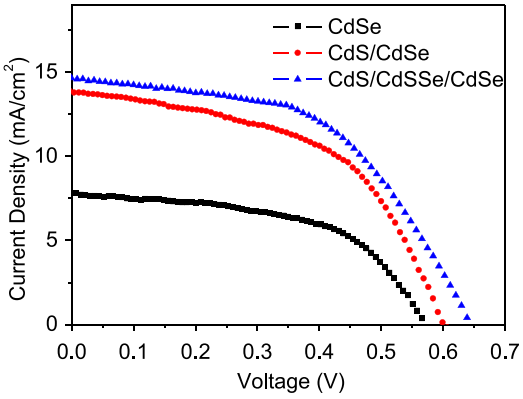

Fig. 9. Current density-voltage (*J-V*) characteristics of CdSe, CdS/CdSe and CdS/CdSSe/CdSe QDSCs measured under the illumination of one sun (AM 1.5, 100 mW cm^{-2}).

Table 3
Photovoltaic parameters of CdSe, CdS/CdSe and CdS/CdSSe/CdSe QDSCs.

Sample	J_{sc} (mA cm^{-2})	V_{oc} (V)	FF	η (%)
CdSe	7.78(± 0.18)	0.57(± 0.01)	0.55(± 0.01)	2.44(± 0.10)
CdS/CdSe	13.88(± 0.22)	0.60(± 0.01)	0.53(± 0.01)	4.41(± 0.13)
CdS/CdSSe/CdSe	14.65(± 0.20)	0.64(± 0.01)	0.54(± 0.01)	5.06(± 0.12)

That is, with respect to that of CdS/CdSe, the incorporated CdSSe layer between CdS and CdSe should take the responsibility for the performance enhancement of the CdS/CdSSe/CdSe device in view of the facilitated charge injection and suppressed charge recombination, and these two considerable effects are schematically illustrated in panel (a) and (b) of Fig. 10 as follows, respectively. Firstly, as is well known for CdS/CdSe band lineup, the redistribution of the electrons between CdS and CdSe is supposed to trigger a downward and upward shift of the band edges, respectively, for CdS and CdSe, which is known as the Fermi level alignment [7,40]. Therefore, the resulting band edges are inferred to have a stepwise structure as schematically shown in panel (a), although the exact band lineups are not very clear in our case because of the high pH of the polysulfide electrolyte, which has been reported to make the TiO_2 bands shift negatively to a greater extent than the corresponding shifts of CdS or CdSe QDs [41]. It is generally believed that the insertion of a CdS layer between TiO_2 and CdSe elevates the conduction band edge of CdSe, giving a higher driving force for the injection of excited electrons out of CdSe layer. Analogously, with incorporation of the CdSSe layer, a similar band edge structure can also be proposed for CdS, CdSSe and CdSe, as demonstrated in the schematic drawing. The conduction and valence band edges of the three materials exerts the increasing order of CdS < CdSSe < CdSe, and such a band alignment is conducive to both electron injection and hole recovery for all the three absorber layers. That is, a ladder-like energy structure suitable for carrier transfer is attained with the incorporation of CdSSe interlayer. Secondly, different from dye molecules, there exist unwanted interfacial defects at the contact interface between QD sensitizers, especially for that of multi-layered QDs, which may inevitably be prone to interphase strain between different QD layers [42,43]. As illustrated in panel (b), in comparison with CdS/CdSe, reduced defects and interphase strain between CdS core and CdSe shell layers should be attained for the CdS/CdSSe/CdSe structure, in which the incorporated CdSSe interlayer

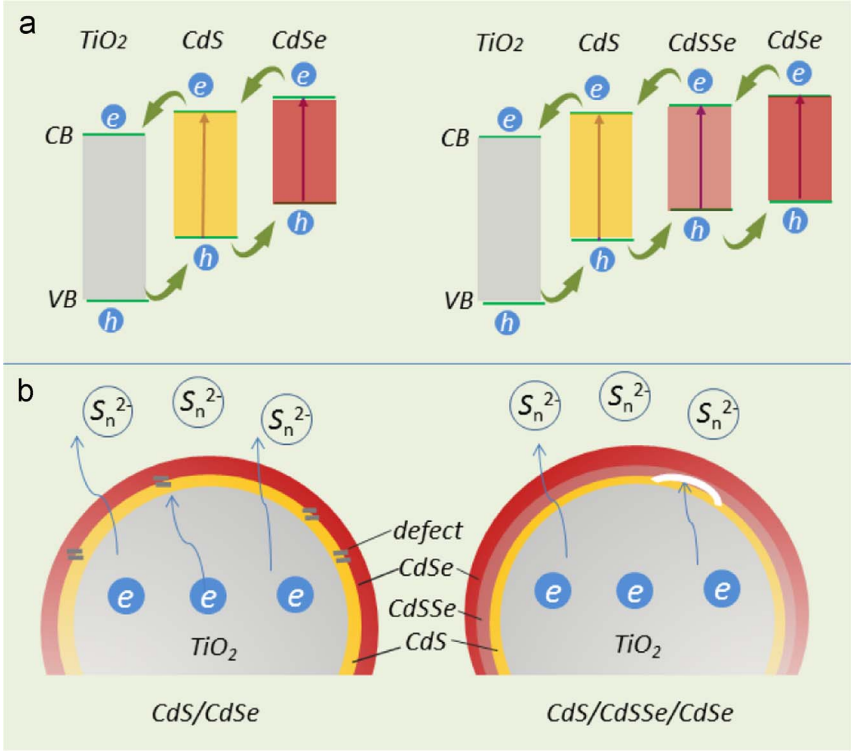

Fig. 10. Schematic diagrams (a) depicting the stepwise band structure of CdS/CdSe and CdS/CdSSe/CdSe for facilitated charge injection, and (b) highlighting the effect of the CdSSe interlayer on suppressing interface charge recombination.

play a positive effect to gradually change the composition of coated QDs. Thanks to the decreased recombination center and favorable band structure, the charge recombination process is significantly suppressed for CdS/CdSSe/CdSe cell, concurring with the EIS measurements. The suppressed charge recombination contributes to the high V_{oc} up to 0.64 V. Therefore, the incorporation of CdSSe interlayer not only forms a favorable stepwise alignment of band-edge levels, which is advantageous to the electron injection, but also plays a complementary effect in passivating the recombination center at the contact interface for retarded charge recombination. As a result, an enhanced photovoltaic performance is achieved for CdS/CdSSe/CdSe QDSC, compared to the conventional CdS/CdSe one.

4. Conclusion

The present work has shown that ternary alloyed QDs provide an effective and reliable approach in selecting desirable properties for developing high-performance photovoltaic devices. In addition to size, ternary QDs make composition as an additional dimension for tailoring the optical and electronic properties, different from that of the widely used binary semiconductors. The excellent ternary CdS_xSe_{1-x} QDs are demonstrated to be efficient sensitizers for QDSCs, and an appropriate bandgap is desired to sufficiently match the solar spectrum for broad light harvesting and achieve ideal band alignment for efficient charge separation. Furthermore, the engineered CdS_xSe_{1-x} QDs were incorporated into CdS/CdSe co-sensitization system as an interlayer for enhanced photovoltaic performance. The incorporated CdS_xSe_{1-x} layer between CdS core and CdSe shell not only helps to construct an efficient band structure facilitating charge injection but also effectively impairs the interfacial defects and interphase strain at CdS/CdSe interface for suppressed charge recombination. Eventually, an improved PCE up to 5.06% is achieved for CdS/CdSSe/CdSe multilayer structure, significantly higher than 4.41% for the conventional CdS/CdSe one. Therefore, with the construction of solar cells employing ternary alloyed QDs, impressive cell performances are achievable with respect to those of the constituent binary systems.

Acknowledgments

This work was financially supported by the National Natural Science Foundation (NSF) of China (No. 51372061 and 51302057) and the Fundamental Research Funds for the Central Universities (No. 2016HGTA0699, 2014HGBZ0334 and 2015HGQC0200). This work was also supported in part by the National Science Foundation (DMR 1035196) and the University of Washington TGIF grant. R. Zhou also gratefully acknowledges a fellowship from the China Scholarship Council.

Appendix A. Supplementary material

Supplementary data associated with this article can be found in the online version at http://dx.doi.org/10.1016/j.solmat.2016.04.049.

References

[1] M. Grätzel, The light and shade of perovskite solar cells, Nat. Mater. 13 (2014) 838–842.
[2] J.J. Tian, G.Z. Cao, Control of nanostructures and interfaces of metal oxide semiconductors for quantum-dots-sensitized solar cells, J. Phys. Chem. Lett. 6 (2015) 1859–1869.
[3] Y. Shirasaki, G.J. Supran, M.G. Bawendi, V. Bulović, Emergence of colloidal quantum-dot light-emitting technologies, Nat. Photonics 7 (2013) 13–23.
[4] Z.X. Pan, I. Mora-Seró, Q. Shen, H. Zhang, Y. Li, K. Zhao, J. Wang, X.H. Zhong, J. Bisquert, High-efficiency "green" quantum dot solar cells, J. Am. Chem. Soc. 136 (2014) 9203–9210.
[5] P.V. Kamat, K. Tvrdy, D.R. Baker, J.G. Radich, Beyond photovoltaics: semiconductor nanoarchitectures for liquid-junction solar cells, Chem. Rev. 110 (2010) 6664–6688.
[6] P.K. Santra, P.V. Kamat, Mn-doped quantum dot sensitized solar cells: a strategy to boost efficiency over 5%, J. Am. Chem. Soc. 134 (2012) 2508–2511.
[7] Y.L. Lee, Y.S. Lo, Highly efficient quantum-dot-sensitized solar cell based on co-sensitization of CdS/CdSe, Adv. Funct. Mater. 19 (2009) 604–609.
[8] J. Wang, I. Mora-Sero, Z.X. Pan, K. Zhao, H. Zhang, Y.Y. Feng, G. Yang, X.H. Zhong, J. Bisquert, Core/shell colloidal quantum dot exciplex states for the development of highly efficient quantum-dot-sensitized solar cells, J. Am. Chem. Soc. 135 (2013) 15913–15922.
[9] Z.X. Pan, K. Zhao, J. Wang, H. Zhang, Y.Y. Feng, X.H. Zhong, Near infrared absorption of $CdSe_xTe_{1-x}$ alloyed quantum dot sensitized solar cells with more than 6% efficiency and high stability, ACS Nano 7 (2013) 5215–5222.
[10] J.J. Tian, Q.F. Zhang, E. Uchaker, R. Gao, X.H. Qu, S.G. Zhang, G.Z. Cao, Architectured ZnO photoelectrode for high effciency quantum dot sensitized solar cells, Energy Environ. Sci. 6 (2013) 3542–3547.
[11] J.J. Tian, Q.F. Zhang, L.L. Zhang, R. Gao, L.F. Shen, S.G. Zhang, X.H. Qu, G.Z. Cao, ZnO/TiO_2 nanocable structured photoelectrodes for CdS/CdSe quantum dot co-sensitized solar cells, Nanoscale 5 (2013) 936–943.
[12] R. Zhou, H.H. Niu, Q.F. Zhang, E. Uchaker, Z.Q. Guo, L. Wan, S.D. Miao, J.Z. Xu, G.Z. Cao, Influence of deposition strategies on CdSe quantum dot-sensitized solar cells: a comparison between successive ionic layer adsorption and reaction and chemical bath deposition, J. Mater. Chem. A 3 (2015) 12539–12549.
[13] R. Zhou, Q.F. Zhang, J.J. Tian, D. Myers, M. Yin, G.Z. Cao, Influence of cationic precursors on CdS quantum-dot-sensitized solar cell prepared by successive ionic layer adsorption and reaction, J. Phys. Chem. C 117 (2013) 26948–26956.
[14] R. Zhou, Q.F. Zhang, E. Uchaker, J.L. Lan, M. Yin, G.Z. Cao, Mesoporous TiO_2 beads for high efficiency CdS/CdSe quantum dot co-sensitized solar cells, J. Mater. Chem. A 2 (2014) 2517–2525.
[15] R. Zhou, Q.F. Zhang, E. Uchaker, L. Yang, N.Q. Yin, Y.H. Chen, M. Yin, G.Z. Cao, Photoanodes with mesoporous TiO_2 beads and nanoparticles for enhanced performance of CdS/CdSe quantum dot co-sensitized solar cells, Electrochim. Acta 135 (2014) 284–292.
[16] X.H. Shen, J.G. Jia, Y. Lin, X.W. Zhou, Enhanced performance of CdTe quantum dot sensitized solar cell via anion exchanges, J. Power Sources 277 (2015) 215–221.
[17] J.-W. Lee, D.-Y. Son, T.K. Ahn, H.-W. Shin, I.Y. Kim, S.-J. Hwang, M.J. Ko, S. Sul, H. Han, N.-G. Park, Quantum-dot-sensitized solar cell with unprecedentedly high photocurrent, Sci. Rep. 3 (2013) 1050.
[18] A.H. Ip, S.M. Thon, S. Hoogland, O. Voznyy, D. Zhitomirsky, R. Debnath, L. Levina, L.R. Rollny, G.H. Carey, A. Fischer, K.W. Kemp, I.J. Kramer, Z.J. Ning, A. J. Labelle, K.W. Chou, A. Amassian, E.H. Sargent, Hybrid passivated colloidal quantum dot solids, Nat. Nanotechnol. 7 (2012) 577–582.
[19] J.J. Tian, L.L. Lv, C.B. Fei, Y.J. Wang, X.G. Liu, G.Z. Cao, A highly efficient (> 6%) $Cd_{1-x}Mn_xSe$ quantum dot sensitized solar cell, J. Mater. Chem. A 2 (2014) 19653–19659.
[20] M.A. Hossain, J.R. Jennings, C. Shen, J.H. Pan, Z.Y. Koh, N. Mathews, Q. Wang, CdSe-sensitized mesoscopic TiO2 solar cells. Exhibiting > 5% efficiency: redundancy of CdS buffer layer, J. Mater. Chem. 22 (2012) 16235–16242.
[21] M.A. Hossain, J.R. Jennings, N. Mathews, Q. Wang, Band engineered ternary solid solution CdS_xSe_{1-x} sensitized mesoscopic TiO_2 solar cells, Phys. Chem. Chem. Phys. 14 (2012) 7154–7161.
[22] A. Braga, S. Giménez, I. Concina, A. Vomiero, I. Mora-Seró, Panchromatic sensitized solar cells based on metal sulfide quantum dots grown directly on nanostructured TiO_2 electrodes, J. Phys. Chem. Lett. 2 (2011) 454–460.
[23] A. Tubtimtae, K.L. Wu, H.Y. Tung, M.W. Lee, G.J. Wang, Ag_2S quantum dot-sensitized solar cells, Electrochem. Commun. 12 (2010) 1158–1160.
[24] X.H. Song, M.Q. Wang, J.P. Deng, Z. Yang, C.X. Ran, X.Y. Zhang, X. Yao, One-step preparation and assembly of aqueous colloidal CdS_xSe_{1-x} nanocrystals within mesoporous TiO_2 films for quantum dot-sensitized solar cells, ACS Appl. Mater. Interfaces 5 (2013) 5139–5148.
[25] W. Ma, J.M. Luther, H. Zheng, Y. Wu, A.P. Alivisatos, Photovoltaic devices employing ternary PbS_xSe_{1-x} nanocrystals, Nano Lett. 9 (2009) 1699–1703.
[26] L. Yang, R. Zhou, J.L. Lan, Q.F. Zhang, G.Z. Cao, J.G. Zhu, Efficient band alignment for $Zn_xCd_{1-x}Se$ QD-sensitized TiO_2 solar cells, J. Mater. Chem. A 2 (2014) 3669–3676.
[27] P.K. Santra, P.V. Kamat, Tandem-layered quantum dot solar cells: tuning the photovoltaic response with luminescent ternary cadmium chalcogenides, J. Am. Chem. Soc. 135 (2013) 877–885.
[28] T. Shu, Z.M. Zhou, H. Wang, G.H. Liu, P. Xiang, Y.G. Rong, H.W. Han, Y.D. Zhao, Efficient quantum dot-sensitized solar cell with tunable energy band $CdSe_xS_{1-x}$ quantum dots, J. Mater. Chem. 22 (2012) 10525–10529.
[29] T.K. Sung, J.H. Kang, D.M. Jang, Y. Myung, G.B. Jung, H.S. Kim, C.S. Jung, Y.J. Cho, J. Park, C.-L. Lee, CdSSe layer-sensitized TiO_2 nanowire arrays as efficient photoelectrodes, J. Mater. Chem. 21 (2011) 4553–4561.
[30] F. Xu, X. Ma, S.M. Kauzlarich, A. Navrotsky, Enthalpies of formation of CdS_xSe_{1-x} solid solutions, J. Mater. Res. 24 (2009) 1368–1374.
[31] J.P. Lu, C. Sun, M.R. Zheng, N. Mathews, H.W. Liu, G.S. Chen, X.H. Zhang, S.G. Mhaisalkar, S.C. Haur, Facile one-step synthesis of CdS_xSe_{1-x} nanobelts with uniform and controllable stoichiometry, J. Phys. Chem. C 115 (2011) 19538–19545.

[32] R. Xie, U. Kolb, J. Li, T. Basché, A. Mews, Synthesis and characterization of highly luminescent CdSe-core CdS/$Zn_{0.5}Cd_{0.5}$S/ZnS multishell nanocrystals, J. Am. Chem. Soc. 127 (2005) 7480–7488.
[33] M.D. Hernández-Alonso, F. Fresno, S. Suárez, J.M. Coronado, Development of alternative photocatalysts to TiO_2: challenges and opportunities, Energy Environ. Sci. 2 (2009) 1231–1257.
[34] Y. Choi, M. Seol, W. Kim, K. Yong, Chemical bath deposition of stoichiometric CdSe quantum dots for efficient quantum-dot-sensitized solar cell application, J. Phys. Chem. C 118 (2014) 5664–5670.
[35] K.Y. Yan, W. Chen, S.H. Yang, Significantly enhanced open circuit voltage and fill factor of quantum dot sensitized solar cells by linker seeding chemical bath deposition, J. Phys. Chem. C 117 (2013) 92–99.
[36] X.Y. Yu, J.Y. Liao, K.Q. Qiu, D.B. Kuang, C.Y. Su, Dynamic study of highly efficient CdS/CdSe quantum dot-sensitized solar cells fabricated by electrodeposition, ACS Nano 5 (2011) 9494–9500.
[37] N. Koide, A. Islam, Y. Chiba, L.Y. Han, Improvement of efficiency of dye-sensitized solar cells based on analysis of equivalent circuit, J. Photochem. Photobiol. A 182 (2006) 296–305.
[38] Q. Wang, J.-E. Moser, M. Grätzel, Electrochemical impedance spectroscopic analysis of dye-sensitized solar cells, J. Phys. Chem. B 109 (2005) 14945–14953.
[39] R. Kern, R. Sastrawan, J. Ferber, R. Stangl, J. Luther, Modeling and interpretation of electrical impedance spectra of dye solar cells operated under open-circuit conditions, Electrochim. Acta 47 (2002) 4213–4225.
[40] L. Yang, C. McCue, Q.F. Zhang, E. Uchaker, Y.H. Mai, G.Z. Cao, Highly efficient quantum dot-sensitized TiO_2 solar cells based on multilayered semiconductors (ZnSe/CdS/CdSe), Nanoscale 7 (2015) 3173–3180.
[41] O. Niitsoo, S.K. Sarkar, C. Pejoux, S. Rühle, D. Cahen, G. Hodes, Chemical bath deposited CdS/CdSe-sensitized porous TiO_2 solar cells, J. Photochem. Photobiol. A 181 (2006) 306–313.
[42] J. Kim, H. Choi, C. Nahm, C. Kim, J.I. Kim, W. Lee, S. Kang, B. Lee, T. Hwang, H.H. Park, B. Park, Graded bandgap structure for PbS/CdS/ZnS quantum-dot-sensitized solar cells with a $Pb_xCd_{1-x}S$ interlayer, Appl. Phys. Lett. 102 (2013) 183901.
[43] T. Moon, J.H. Jun, H. Lee, W. Yoon, S. Kim, B.-K. Lee, H.-C. Lee, W. Kim, S.-H. Ahn, S. Lee, H.-M. Lee, Additional coating effects on textured ZnO:Al thin films as transparent conducting oxides for thin-film Si solar cells, Prog. Photovolt. 20 (2012) 294–297.